CONF-8809322--2

MODELING DISLOCATION EVOLUTION IN IRRADIATED ALLOYS*

R. E. Stoller

Metals and Ceramics Division
Oak Ridge National Laboratory
P.O. Box 2008
Oak Ridge, TN 37831-6376

CONF-8809322--2

DE90 004921

ABSTRACT

Neutron irradiation of structural materials leads to such observable changes as creep and void swelling. These effects are due to differential partitioning of point defects. Although most radiation-produced point defects recombine with an antidefect, a very small fraction of the defects survive. The surviving defect fraction is directly related to the density and type of extended defects that act as point defect sinks. Defect partitioning requires the presence of more than one type of sink and that at least one of the sinks has a capture efficiency for either vacancies or interstitials that is different from that of the other sink(s). For example, dislocations provide the interstitial "bias" that drives swelling and the ratio of the dislocation to cavity sink strength determines the swelling rate. These sink strengths change during irradiation and an explicit model of their evolution is required to simulate swelling or creep. Such a model has been developed; the influence of various model assumptions and parameters is discussed. The model simulates the evolution of Frank faulted interstitial loops, providing a dislocation source and the glide/climb of the dislocation network leading to annihilation of dislocation segments. Good agreement is found between model predictions and experimental data. Swelling simulations are shown to be quite sensitive to the dislocation model.

*Research sponsored by the Office of Fusion Energy and the Division of Materials Sciences, U.S. Department of Energy, under contract DE-AC05-84OR21400 with Martin Marietta Energy Systems, Inc.

MODELING DISLOCATION EVOLUTION IN IRRADIATED ALLOYS*

R. E. Stoller

Metals and Ceramics Division
Oak Ridge National Laboratory
P.O. Box 2008
Oak Ridge, TN 37831-6376

1. INTRODUCTION

Dislocations are responsible for much of the observed mechanical behavior of structural materials. The generation and motion of dislocations permits materials to deform plastically without fracturing and the detailed stress-strain behavior of materials can be correlated with the evolution of the dislocation structure. At high temepratures, dislocation motion and the ability of dislocations to act as vacancy sources and sinks have a major influence on the creep behavior of materials. Dislocations also play a major role in determining the response of materials to displacive irradiation. When structural materials are irradiated with high energy neutrons or charged particles, higher-than-equilibrium concentrations of both vacancies and interstitials are obtained. Most of these radiation-produced point defects recombine with an antidefect; but, a very small fraction of the defects survive. Their survival leads to such observable effects of radiation as void swelling and irradiation creep. The surviving defect fraction is directly related to the density and type of extended defects that act as point defect sinks.

In particular, differential partitioning of the two types of point defects is required in order to obtain a net change in the microstructure of irradiated materials. This in turn requires that there exist more than one type of sink, and that at least one of the sinks has a capture efficiency for either vacancies or interstitials that is different from that of the other sink(s). One example of this differential partitioning is that which arises due to the interaction of the long range strain fields of dislocations and interstitials. Because of this interaction, dislocations have a larger capture efficiency for interstitials

*Research sponsored by the Office of Fusion Energy and the Division of Materials Sciences, U.S. Department of Energy, under contract DE-AC05-84OR21400 with Martin Marietta Energy Systems, Inc.

than they do for vacancies and the dislocation capture efficiency for interstitials exceeds that of cavities for interstitials. These two capture efficiency differences provide the interstitial "bias" that drives void nucleation and growth in irradiated materials. The ratio of the dislocation to cavity sink strength has a significant impact on void nucleation and this ratio largely determines the swelling rate at steady state. This concept is discussed in detail by Lee and Mansur [1]. Since these sink strengths change during irradiation, an explicit model of their evolution is required to simulate swelling or creep.

A model of dislocation evolution based on the reaction rate theory has been developed and coupled with a model of cavity evolution that has been shown to give good quantitative agreement with void swelling data [2-4]. The results presented here use a model which is an extension and modification of earlier work by Stoller and Odette [4]. The dislocation model simulates the evolution of a pre-existing dislocation structure due to purely thermal effects as well as the Frank faulted interstitial loops that are formed during irradiation. These loops provide a source of network dislocations and the glide/climb of the dislocation network simultaneously leads to its annihilation.

2. MODEL DESCRIPTION

The model that has been developed includes components to simulate both thermal and radiation-induced mechanisms. Thermally-activated Bardeen-Herring sources provide a source of line dislocations at high temperatures, while climb and glide processes can lead to the simultaneous annihilation of line dislocation segments that have opposing Burger's vectors. The model assumes that dislocation climb is the rate controlling process. In the absence of displacive irradiation, dislocation climb is assumed to be driven by stress-directed preferential thermal emission of vacancies. Similar models have been developed previously for the study of creep processes [5,6]. Displacive irradiation provides an additional source of line dislocations through the formation and

evolution of Frank faulted dislocation loops, and the higher-than-equilibrium levels of point defects alter the dislocation climb rate.

Thermally-Activated Components of Dislocation Model

The climb velocity of an edge dislocation can be written as:

$$v_{cl} = \frac{2\pi}{\ln(r_o/r_c)} \frac{1}{b_n} \left[Z_i^n D_i C_i - Z_v^n D_v (C_v - C_v^n) \right] \quad (1)$$

where $D_{i,v}$ and $C_{i,v}$ are the diffusivities and atomic concentrations of interstitials and vacancies, the $Z_{i,v}^n$ are the dislocation capture efficiencies for interstitials and vacancies, b_n is the Burger's vector of a line dislocation, r_c is the dislocation core radius, r_o is the outer radius of the cylindrical cell used in calculating the dislocation sink strength [2,4,7], and C_v^n is the concentration of vacancies in equilibrium with the dislocation. In the absence of irradiation C_i is negligible and C_v is close to the themal equilibrium vacancy concentration, C_v^e. In this case Equation (1) reduces to a simpler form that has been used by others (see, for example Nix, et al. [8]). The concentration C_v^n is a function of any applied or internal stress and is given by

$$c_v^n = C_v^e \exp\left(\frac{\sigma\Omega}{kT}\right) \quad (2)$$

where σ is the net tensile stress, Ω is the atomic volume, and kT has its usual meaning.

Adopting the model of Gibbs [9], an internal (back) stress is assumed to exist as the result of a population of immobilized dislocations

$$\sigma = AGb_n \rho_p^{1/2} \quad , \quad (3)$$

where G is the shear modulus and A is a geometric parameter with a nominal value of 0.4. The density of pinned dislocations, ρ_p, in Equation (3) is assumed to be a constant fraction of the total network dislocation density, and this fraction is treated here as an adjustable parameter.

The average distance that a network dislocation can climb before annihilating with another one is taken as the equivalent radius of a volume-conserving dislocation cell.

$$d_{cl} = (\pi\rho_n)^{-1/2} \quad . \tag{4}$$

Equations (1) to (4) can then be used to obtain a mean lifetime against annihilation due to this climb-glide process as

$$\tau_{cl} = d_{cl}/v_{cl} \tag{5}$$

The dislocation network can also be regenerated as the result of sources that act by dislocation climb and from the emission of dislocations at precipitate interfaces. Since it would be difficult to describe these dislocation generation processes in detail, a simple model was developed for the generation of network dislocations by the so-called Bardeen-Herring sources [10]. Bardeen-Herring sources are similar to Frank-Read sources except that the former are climb-driven while the latter are glide-driven. Such a source is shown schematically in Figure 1 in which a pinned dislocation segment is bowed due to an applied stress. After climbing a sufficient distance, the source will collapse leaving a dislocation loop and the original line segment once again able to generate succeeding loops. For simplicity, the source may be assumed to generate $2\pi L$ of new dislocation line length after climbing a distance L. The time to generate this new line length (τ_{BH}) is defined by analogy to Equation (5). The climb velocity is again given by Equation (1) and the generation rate is then

$$R_{BH} = \frac{2\pi L}{\tau_{BH}} S_{BH} = 2\pi v_{cl} S_{BH} , \qquad (6)$$

in which S_{BH} is the Bardeen-Herring source density.

In earlier work [4], S_{BH} was treated as a temperature-dependent input parameter. Here, the use of a simple explicit relationship between S_{BH} and the dislocation density was sought. Since pinned dislocation segments are required for these sources, they are assumed to be due to the same pinned dislocation density used in Equation (3). In cold-worked materials, the subgrain structure, and the dislocations network can provide sources of this type. If all of the potential sources due to ρ_p were active, the Bardeen-Herring source density would be:

$$S_{BH} = (\rho_p/3)^{1.5} \qquad (7)$$

Equation (7) is based on the number nodes or intersection points that would be formed by a uniformly distributed, isotropic, three-dimensional array of ρ_p line dislocations.

The thermal dislocation source and annihilation terms were calibrated using tensile data obtained at 450, 550 and 650°C for AISI 316 stainless steel. This data included yield strength measurements (2% offset) for both 20% cold-worked and solution-annealed material, as well as 20% cold-worked material aged for 4000 hours at the test temperature [11]. Assuming that the hardening increment due to network dislocations varies as $(\rho_n)^{1/2}$ and that this is the primary cause of the increased yield strength of the cold-worked material relative to the solution-annealed material, the ratios shown in Table 1 are obtained from the data. The model's predictions for these same ratios are also listed. These were obtained by computing the dislocation evolution with the atomic displacement rate set to zero in the model. The predicted values are also consistent with transmission electron microscope observations on the same heat of steel after thermal aging [12]. The predicted thermal behavior of the network

dislocation density for initially 20%-cold-worked material is shown in Figure 2 as a function of the thermal annealing time and temperature. These predictions are also broadly consistent with observed behavior. Little recovery takes place below about 600°C, even for long annealing times; while almost complete recovery is predicted after one hour at 1050°C. The parameters used to obtain these results are listed in Table 2.

Radiation-Induced Dislocation Processes

In order for the model to include the time dependence of the dislocation structure, the standard rate equations used to obtain the vacancy and interstitial concentrations are modified to include the influence of di-, tri-, and tetra-interstitial clusters [2,4]. Additional rate equations describe these interstitial cluster concentrations. The concentrations of the point defects and the interstitial clusters are calculated at steady-state and only the mono-defects are assumed to be mobile. The tetra-interstitial is considered to be the stable nucleus for Frank faulted loop formation. If a discrete clustering calculation was used to describe the full size range of the experimentally observed loop population, the number of rate equations required would exceed ten thousand. Therefore a practical method was developed to discretize the continuum distribution of loops larger than the tetra-interstitial. It has been shown in previous work [4] that this method of joining a set of discrete interstitial cluster equations to a multi-size-class description of the loop population provides an adequate mathematical representation of the loop nucleation process. Figure 3 is reproduced from Reference 3 and shows the dependence of the Frank faulted loop density and the loop line length as a function of the number of loop size classes used. Only a modest number of size classes is required to insure that the results are independent of the number of size classes.

Under irradiation, the growth and unfaulting of Frank loops provide an additional source of network dislocations. The radial growth velocity of a faulted loop is given by an equation analogous to Equation (1), with values of

the capture efficiencies, Burger's vector, and equilibrium vacancy concentration appropriate for the loops [4]. The loop size space is divided up into a number of size classes and the time constant for growth between size classes with radii r_ℓ^j and r_ℓ^{j+1} is:

$$\tau_j = \int_{r_\ell^j}^{r_\ell^{j+1}} \left\{ \frac{2\pi}{\ell n(r_o/r_c)} \left[Z_i^\ell D_i C_i - Z_V^\ell D_V (C_V - C_V^\ell) \right] \right\}^{-1} dr \qquad (8)$$

where the integrand is the loop radial growth velocity. The number of loops in the j-th size class (N_ℓ^j) is then governed by the following equation:

$$\frac{dN_\ell^j}{dt} = N_\ell^{i-1} \tau_i^{-1} - N_\ell^i \tau_{i+1}^{-1} \qquad (9)$$

The maximum loop size is assumed to be limited by a simple geometrical constraint, namely that the loop will unfault when it impinges on another loop or network dislocation due to the interaction of their strain fields [13]. Hence

$$r_\ell^{max} = (\pi \rho_t)^{-1/2} , \qquad (10)$$

where ρ_t is the total (i.e. Frank loop line length plus network) dislocation density. As the loops grow into this size class, they are no longer considered to be Frank loops and an equivalent quantity of dislocation line length $2\pi r_\ell^{max} N_\ell^{max}$ is added to the dislocation network. The rate at which new dislocation line length is generated by this mechanism is:

$$R_{FL} = 2\pi r_{\ell}^{max} N_{\ell}^{max} \tau_{max}^{-1} \quad . \tag{11}$$

As mentioned above, the additional point defects generated by irradiation alter the dislocation climb velocity given in Equation (1). Using Equations (1) and (5) to (9), the rate equation describing the evolution of the dislocation network is obtained as

$$\frac{d\rho_n}{dt} = 2\pi(v_{cl} S_{BH} + r_{\ell}^{max} N_{\ell}^{max} \tau_{max}^{-1}) - \rho_n \tau_{cl}^{-1} \tag{12}$$

Cavity Evolution Model

The details of the cavity evolution component of the model used here have been discussed in detail elsewhere [2,3,14], so only a brief summary will be given here. The work discussed in References 2, 3 and 15 helped to establish what has become the generally accepted sequence of events that are reponsible for void swelling in irradiated materials. Gas-stabilized, near equilibrium bubbles form at very low doses. In the absence of the stabilizing gas, vacancy emission would cause these bubbles to shrink. Helium produced by transmutation reactions is believed to be the most significant gas in this respect. Voids are formed as a result of the growth of these bubbles to a critical size beyond which the bubbles are thermodynamically unstable, ie. vacancy emission is more than balanced by vacancy absorption and additional gas is no longer required to maintain growth. These supercritical cavities are referred to as voids since the gas pressure within them becomes much less than the equilibrium pressure as they grow. Similar theoretical work by others has confirmed this scenario [15-17].

The size of the bubbles is calculated as a function of their helium content and the effective vacancy supersaturation using the procedures described in Reference 14. After the bubbles in a given size class reach the critical size and convert to voids, their radius (r_c) is calculated by integrating the equation that describes the instantaneous radial growth velocity:

$$\frac{dr_c}{dt} = \frac{1}{r_c}\left[Z_v^c D_v (C_v - C_v^c) - Z_i^c D_i C_i\right] \tag{13}$$

in which Z_i^c and Z_v^c are the cavity capture efficiencies for interstitials and vacancies and C_v^c is the vacancy concentration in equilibrium with a cavity with radius r_c [14].

DISCUSSION OF MODEL PREDICTIONS

One goal of developing models such as that described above is to try and gain an understanding of the important physical processes that lead to microstructural evolution under irradiation. The need to provide some predictive capability is a second motivation. Simple void swelling models have been successfully used to explain much of the available swelling data and have provided considerable insight into the mechanisms responsible for this phenomenon [2-4, 14-19]. Unfortunately, the ability to use these models in a predictive way is compromised by at least two problems. One is uncertainties in the values of the major material parameters for engineering alloys that these models require. In some cases, measurements made on pure metals can be used to provide initial estimates, but key parameters are known to be sensitive to alloy composition and perhaps impurities [20-25]. A second problem is that the assumptions required to implement the simple models renders them insensitive to certain material parameters and in some cases requires that the dose dependence of some of the microstructural components be neglected.

For example, one limiting case that is frequently examined using the rate theory is to ignore bulk recombination and assume that dislocations are the major point defect sink. In this case, the effective vacancy supersaturation takes the following simple form [18].

$$\Phi = \frac{\eta\, G_{dpa}}{S_i^n D_v C_v^e}\left(Z_i^n - 1\right) , \tag{14}$$

where $D_v C_v^e$ is the self-diffusion coefficient, S_i^n is the dislocation sink strength, G_{dpa} is the displacement rate. Values of the cascade efficiency (η) between 0.1 and 1.0 have been used by various workers [2,26,27] and values of the dislocation capture efficiency for interstitials (Z_i^n) have varied from ~1.02 to > 1.5 [2,28,29]. Depending on the values chosen for these two parameters, the computed supersaturation can vary significantly. Since the critical bubble radius is proportional to the reciprical of the effective supersaturation, the predicted inclubation time for void swelling is strongly affected by the parametric uncertainties. In practice, estimates of these parameters have frequently been made using the results of radiation experiments. Unless the sink structure is known at the time that the bubbles are converting to voids, such estimates of the parameters must be viewed as highly uncertain.

Figure 4 provides an example of the significance of using a model in which the dose dependence of the dislocation structure is explicitly included. This Figure compares the predicted void swelling as a function of irradiation dose for various assumed dislocation densities at 400 and 500°C. For both temperatures, the results of the present model with the time (dose) dependent dislocation density are compared with results obtained with three time-independent values. The values of 6.37×10^{14} and 1.95×10^{14} m^{-2} are the values that obtained at high doses in the present model at 400 and 550°C respectively. The other two values (5.0×10^{14} and 3.0×10^{15} m^{-2}) are used to help show the sensitivity of the predicted swelling to what has been termed a typical "steady-state" value in this temperature range [30] and the initial, as-cold-worked value. Significant variations in the incubation time and swelling rate are observed in Figure 4. The behavior at 400°C is particularly complex. This effect is due to the balance of point defect partitioning between the network dislocations and the other micro-structural sinks. When the dislocations are the dominant sink, increases in the dislocation density reduce the vacancy supersaturation. This increases the critical bubble size and extends the incubation time for void swelling. The influence of the dislocation/interstitial bias is less significant because most point defects are recombining at the

dislocations. On the other hand, when dislocations are not the dominant sink, an increased dislocation density will result in an increased supersaturation. This is shown in Figure 5 where the effective vacancy supersaturation is plotted as a function of the dislocation density for 400 and 550°C.

$$\Phi = \frac{Z_v^c D_v C_- Z_i^c D_i C_i}{Z_v^c D_v C_v^e} \tag{15}$$

The nonmonotonic swelling behavior with dislocation density at 400°C shown in Figure 4a is a result of the maximum in the effective supersaturation at $\sim 1 \times 10^{15} m^{-2}$ shown in Figure 5. This result emphasizes the importance of using appropriate temperature, as well as dose, dependent values for the various sink parameters in modeling studies.

A second attractive feature of the more comprehensive model described here is that it exhibits an increased sensitivity to parameter variations when compared to simpler models that neglect dislocation evolution. For example, Equation 14 indicates that for any mechanism that is dependent on the vacancy supersaturation, e.g. void formation, relative changes in Z_i^η and η can be used to offset one another in a simple model. This is no longer the case in the present model since the evolution of the various sinks exhibit different dependencies on these parameters. The cavity and dislocation evolution are not independent but are coupled in a complex way via their mutual effect on the point defect concentrations as shown in Figure 4.

The dependence of the model's predictions on the interstitial migration energy, E_i^m, provides another example of increased parametric sensitivity. The values of most of the parameters listed in Table 2 generally fall within the range of what might be termed "typical" for the void swelling models which have been referred to above. The relatively high value for E_i^m is a notable

exception. Measurements of E_i^m in pure metals have generally led to the use of lower values, <0.5 eV [31]. However, the results obtained from these simple void swelling models are not sensitive to the value of E_i^m [32]. The results obtained with the present model are dependent on E_i^m via its influence on the predicted faulted loop population and their subsequent effect on network dislocation density. The sensitivity of the model's predictions to E_i^m is shown in Figure 6. Figure 6a shows that the use of the lower, pure material value for E_i^m results in faulted loop densities which are much lower than is experimentally observed [13,33-36]. This reduced loop density leads to a lower network dislocation density (Figure 6b) since the source term is reduced. The predicted swelling at 100 dpa is reduced in this case (Figure 6c). However, the fluence and temperature dependence of the effect is complex and for any given temperature and dose the predicted swelling may either increase or decrease. The value of Eim=0.85 eV given in Table 2 is in agreement with recent measurements of this parameter in austenitic steels [20,21]. Assuming that these latter measurements are valid, the fact that the model requires such a value for E_i^m is encouraging. Although the present model required the use of additional material parameters as more physical mechanisms were included, the model also became somewhat "stiffer" with respect to arbitrary parameter choices.

Typical results obtained with the present model are shown in Figure 7 where the fluence dependence of the predicted microstructural parameters for solution annealed (a) and 20% cold worked (b) material are compared. The coupling of the evolution of the various microstructural features is clearly seen. After an initial transient the microstructure reaches a state which is independent of the initial condition. The incubation time for swelling is not primarily associated with the dislocation transient but rather with the time required for the cavities to accumulate the critical number of helium atoms. Following the initation of void swelling, some additional network recovery occurs as the cavity sink strength begins to increase. The higher cavity sink strength permits more efficient differential partitioning of point defects, i.e., excess interstitials to dislocations and vacancies to voids [1]. This reduces the amount of point defect recombination at dislocations so that the additional network recovery takes place by interstitial-driven climb. The somewhat lower network dislocation

density permits a slight increase in loop formation, and a new microstructural balance is obtained. A regime in which the swelling rate is approximately constant and fairly high occurs when the cavity and dislocation sink strengths have similar values. When such parity occurs the maximum theoretical swelling rate is observed [37]. While it is not shown in Figure 7, at high doses the cavity sink strength exceeds the dislocation sink strength and the swelling rate begins to decrease as predicted by theory [37] due to greater point defect recombination at the voids. The near coincidence of the values for the solution annealed and cold-worked material at low doses may be somewhat artificial. The model does not include an explicit cavity nucleation calculation and the same initial cavity densities were used for both materials. Some data indicates that void densities at low doses are higher for solution annealed material [35] and neglecting this difference may influence the model's predictions at low doses. The evolution towards a saturation microstructure shown in Figure 7 has been experimantally observed [30,38]. The predicted peak in the faulted loop number density at low doses in solution annealed material has also been observed [35]. However, Brager and Straalsund have reported similar high values at low doses in 20% cold-worked stainless steel [39], while the model predicts that the high initial dislocation density would suppress loop formation. On the dose scale of Figure 7a, the low-dose transient in the faulted loop density occurs too quickly to be seen. While the recovery of the network dislocation density in the 20% cold-worked material appears to be in agreement with the available data [30,39], the initial transient occurs more quickly than some have observed in solution annealed material [30]. This may be related in part to the simple dislocation recovery model included here. The model implicitly assumes that all of the dislocation line length is homogeneously distributed in the material. Since this is generally not the case, the use of a single "effective" climb distance for network dislocation annihilation is probably insufficient to account for the various spatial orientations of the dislocations in the material.

SUMMARY

A theoretical model has been described that provides a vehicle for studying the evolution of the important microstructural features in fast neutron irradiated stainless steel. The major features of the model's description of dislocation evolution include: Frank faulted loop nucleation and growth to provide a source for network dislocations, network dislocation annihilation via climb/glide processes, and components which describe the thermal evolution of the dislocation network in the absence of irradiation. The model of dislocation evolution was linked to a previously developed model of cavity evolution that had been used to analyze the problem of void swelling. Generally good agreement was shown between model predictions and observations from both thermal annealing and irradiation experiments.

The predictions of the model indicate that the individual features do not evolve independently but are coupled via their mutual influences on the point defect concentrations. While the model incorporates the time dependence of only three major microstructural components (cavities, faulted loops, and network dislocations), good agreement has been obtained between the predictions of the model and experimental observations. One positive aspect of this work was that as more microstructural features were added, the parameter space in which one could obtain "reasonable" results became more limited. The results demonstrate the power of the rate theory as a tool for investigating radiation effects and indicate that more complex models such as the one discussed here should exhibit an improved predictive capability.

REFERENCES

1. E. H. Lee and L. K. Mansur, "Unified Theoretical Analysis of Experimental Swelling Data for Irradiated Austenitic and Ferritic/Martensitic Alloys," presented at the 1988 Fall Meeting of TMS/AIME, September, 1988, Chicago, to be published in *Met. Trans.*

2. R. E. Stoller and G. R. Odette, Effects of Radiation on Materials: 11th International Symposium, ASTM STP 782, H. R. Brager and J. S. Perrin, Eds., American Society of Testing and Materials, Philadelphia, 1982, pp. 275-294.

3. R. E. Stoller and G. R. Odette, Radiation Induced Changes in Microstructure: 13th International Symposium, ASTM STP 955, F. A. Garner, N. H. Packan and A. S. Kumar, Eds., American Society of Testing and Materials, Philadelphia, 1987, pp. 358-370.

4. R. E. Stoller and G. R. Odette, Radiation Induced Changes in Microstructure: 13th International Symposium, ASTM STP 955, F. A. Garner, N. H. Packan and A. S. Kumar, Eds., American Society of Testing and Materials, Philadelphia, 1987, pp. 371-393.

5. F. R. N. Nabarro, Phil. Mag. 16 (1967) 231-237.

6. J. Gittus, Creep, Viscoelasticity and Creep Fracture in Solids, John Wiley and Sons, New York, 1975.

7. A. D. Brailsford and R. Bullough, The Theory of Sink Strengths, AERE Harwell Report TP.854, 1980.

8. W. D. Nix, R. Gasca-Neri, and J. P. Hirth, Phil. Mag. 23 (1971) 1339-1349.

9. G. B. Gibbs, Phil. Mag. 23 (1971) 771-780.

10. J. Bardeen and C. Herring, Imperfections in Nearly Perfect Crystals, W. Schockley (Ed.), John Wiley and Sons, New York, 1952.

11. D. Fahr, E. E. Bloom, and J. O. Stiegler, Irradiation Embrittlement and Creep in Fuel Cladding and Core Components, Proc. of BNES Conf., London, 1972, pp. 167-177.

12. P. J. Maziasz, Alloy Development for Irradiation Performance, Quarterly Progress Report, DOE/ER-0045/7, 1981, pp. 54-97.

13. H. R. Brager, F. A. Garner, and G. L. Guthrie, J. Nucl. Mater. 66 (1977) 181-197.

14. R. E. Stoller and G. R. Odette, J. Nucl. Mater. 131 (1983) 118-125.

15. L. K. Mansur and W. A. Coghlan, J. Nucl. Mater. 119 (1983) 1-25.

16. C. A. Parker and K. C. Russell, Scripta Met. 15 (1981) 643-647.

References (Cont.)

17. G. R. Odette and S. C. Langley, Radiation Effects and Tritium Technology for Fusion Reactors, CONF-750989, Vol. I, 1975, pp. 395-416.

18. G. R. Odette and R. E. Stoller, J. Nucl. Mater. 122&123 (1984) 514-519.

19. R. E. Stoller and G. R. Odette, J. Nucl. Mater. 103&104 (1981) 1361-1365.

20. O. Dimitrov and C. Dimitrov, J. Nucl. Mater. 105 (1982) 39-47.

21. J. T. Stanley and J. R. Cost, J. Phys. F: Met. Phys. 14 (1984) 1801-1810.

22. W. Assassa and P. Guialdenq, Met. Sci. 12 (1978) 123-128.

23. S. J. Rothman, L. J. Nowicki, and G. E. Murch, J. Physics. F: Metal Phys. 10 (1980) 383-398.

24. L. E. Murr, G. I. Wong, and R. J. Horylev, Acta Met. 21 (1973) 593-603.

25. R. E. Schramm and R. P. Reed, Met. Trans. A 6A (1975) 1343-1418.

26. M. R. Hayns, The Transition From Gas Bubble to Void Growth, AERE-R8806, U.K.A.E.A., 1977.

27. J. J. Sniegowski and W. G. Wolfer, Ferritic Alloys for Use in Nuclear Energy Technologies, Proc. of Topical Conf., TMS AIME, New York, 1984, pp. 579-586.

28. M. R. Hayns, J. Gallagher, and R. Bullough, "The Derivation of a Simple Void Swelling Equation for Cold Worked 316 Austenitic Stainless Steel," AERE Harwell Report TP.739, 1978.

29. P. T. Heald, Phil. Mag. 31 (1975) 551-558.

30. H. R. Brager, F. A. Garner, E. R. Gilbert, J. E. Flinn, and W. G. Wolfer, Radiation Effects in Breeder Reactor Structural Materials, Proc. of Int. Conf., TMS AIME, New York, 1977, pp. 727-755.

31. F. W. Young, J. Nucl. Mater. 69&70 (1978) 310-370.

32. L. K. Mansur, J. Nucl. Mater. 83 (1979) 109-127.

33. H. R. Brager and J. L. Straalsund, J. Nucl. Mater. 46 (1973) 124-158.

34. P. J. Barton, B. L. Eyre, and D. A. Stow, J. Nucl. Mater. 67 (1977) 181-197.

35. H. R. Brager, J. Nucl. Mater. 57 (1975) 103-118.

36. E. E. Bloom and J. O. Stiegler, Effects of Irradiation on Substructure and Mechanical Properties of Metals and Alloys, ASTM STP 529, ASTM, 1973, pp. 360-382.

References (Cont.)

37. L. K. Mansur, Nucl. Tech. 40 (1978) 5-34.

38. N. H. Packan and K. Farrell, Effects of Radiation on Materials: Eleventh Int. Symp., ASTM STP 782, 1982, pp. 885-894.

39. H. R. Brager and J. L. Straalsund, J. Nucl. Mater. 47 (1973) 105-109.

LIST OF TABLES

Table 1. Results of thermal dislocation evolution model

Dislocation Density Ratio: $\frac{\text{(Cold-Worked + 4000 hr at T)}}{\text{(As Cold-Worked)}}$

Test Temperature T (°C)	Data	Model
450	0.73	0.99
550	0.41	0.56
650	0.05	0.04

Table 2. Material and irradiation parameters

Displacement rate	1×10^{-6} dpa/sec
Cascade efficiency	0.333
Vacancy migration energy	1.4 eV
Vacancy formation energy	1.6 eV
Interstitial migration energy,	0.85 eV
Binding energies:	
Di-interstitial,	1.35 eV
Tri-interstitial,	1.75 eV
Recombination radius	1.8 nm
Surface free energy	$3.24 - 1.4 \times 10^{-3}$ T(°C) J/m^2
Stacking fault energy	1.5×10^{-2} J/m^2
Initial dislocation density	3.0×10^{15} m^{-2} 20% cold-worked
	3.0×10^{13} m^{-2} solution-annealed
Pinned dislocation fraction	0.1
Interstitial capture efficiencies:	
Network dislocations	1.25
Faulted loops	1.50
Cavities	1.00
Vacancy capture efficiencies:	
Network dislocations	1.00
Faulted loops	1.00
Cavities	1.00

FIGURE CAPTIONS

Figure 1. Schematic drawing of Bardeen-Herring dislocation source (after Ref. 10).

Figure 2. Predicted network dislocation density as a function of thermal annealing time and and annealing temperature.

Figure 3. Dependence of the Frank faulted loop density (N_ℓ) and loop line length (r_ℓ) on the number of loop size classes at 450°C.

Figure 4. Comparison of predicted swelling at 400 (a) and 550°C (b) with dose-dependent and various constant network dislocation densities.

Figure 5. Effect of assumed network dislocation density on the effective vacancy supersaturation at 400 and 550°C.

Figure 6. Influence of the interstitial migration energy on the predicted Frank faulted loop density (a), network dislocation density (b), and swelling (c).

Figure 7. Predicted dose dependence of Frank faulted loop density, network dislocation density, and void swelling at 500°C for solution annealed (a) and 20% cold-worked (b) austenitic stainless steel. Note that the loop density scale in (b) is different than in (a).

ORNL-DWG 85-16835R

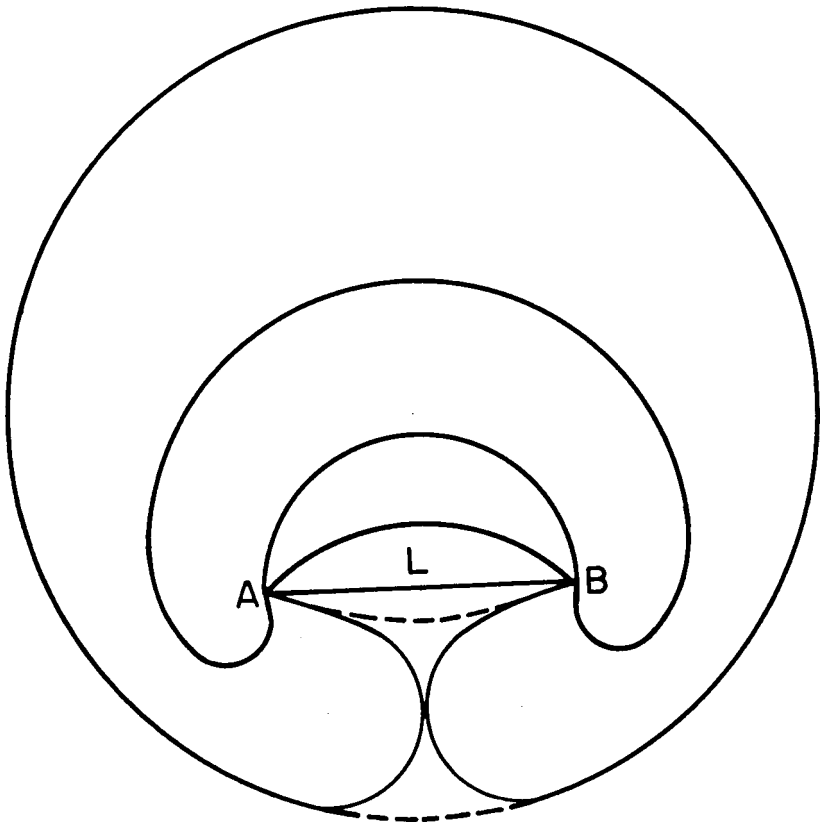

Fig. 1
Stoller

ORNL-DWG 89Z-15936

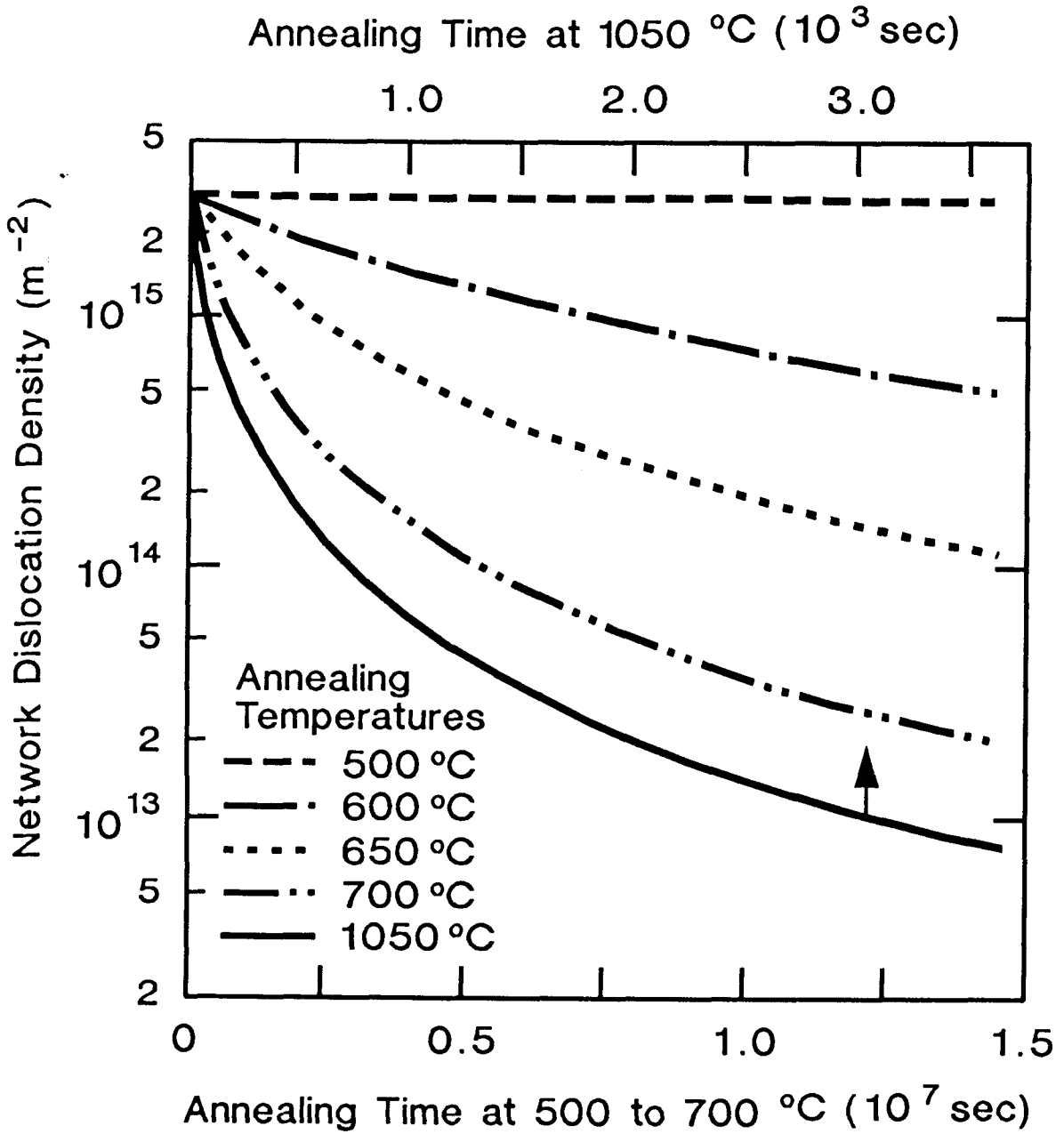

Fig 2
Stoller

ORNL-DWG 85-16836

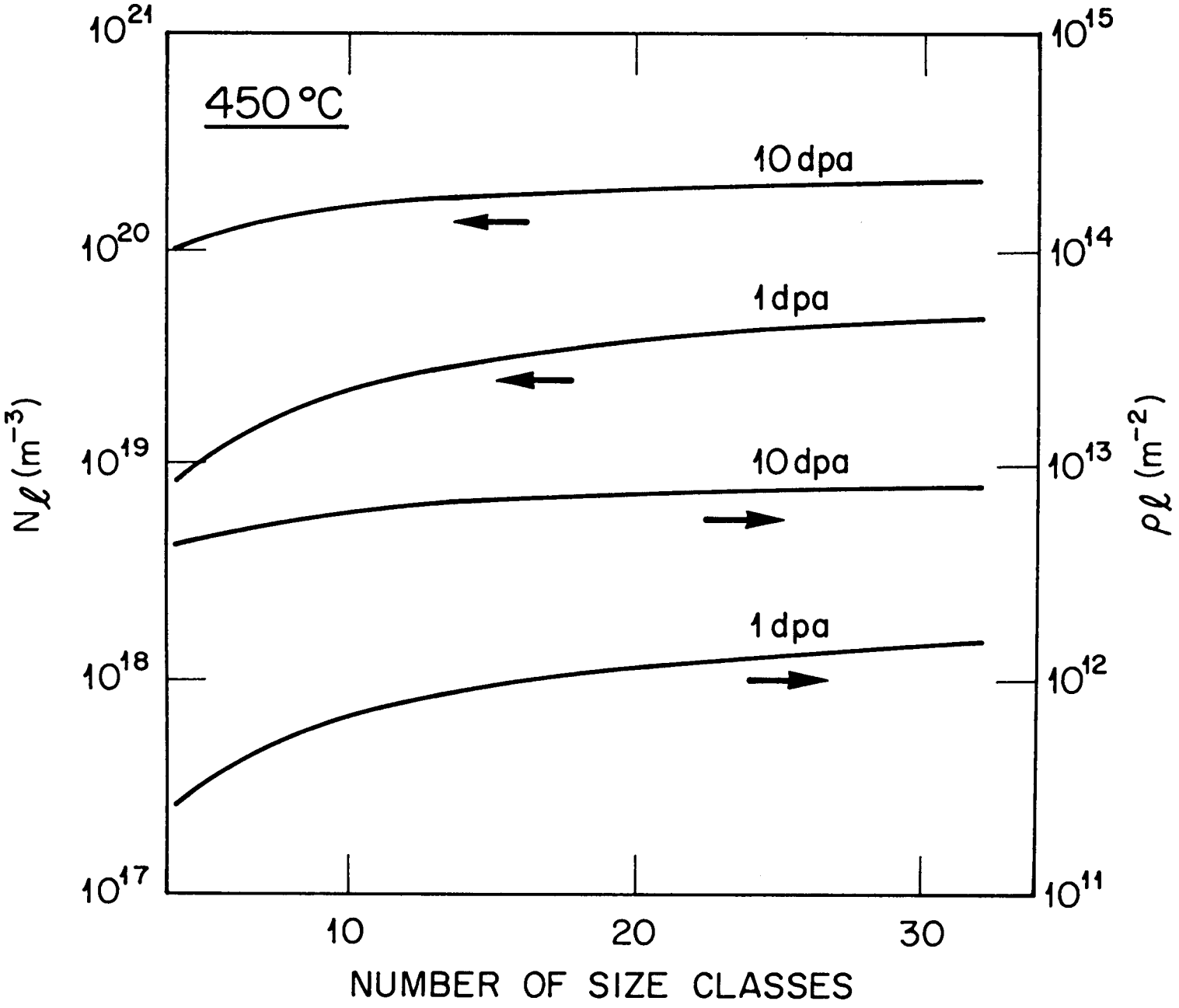

Fig 3
Stoller

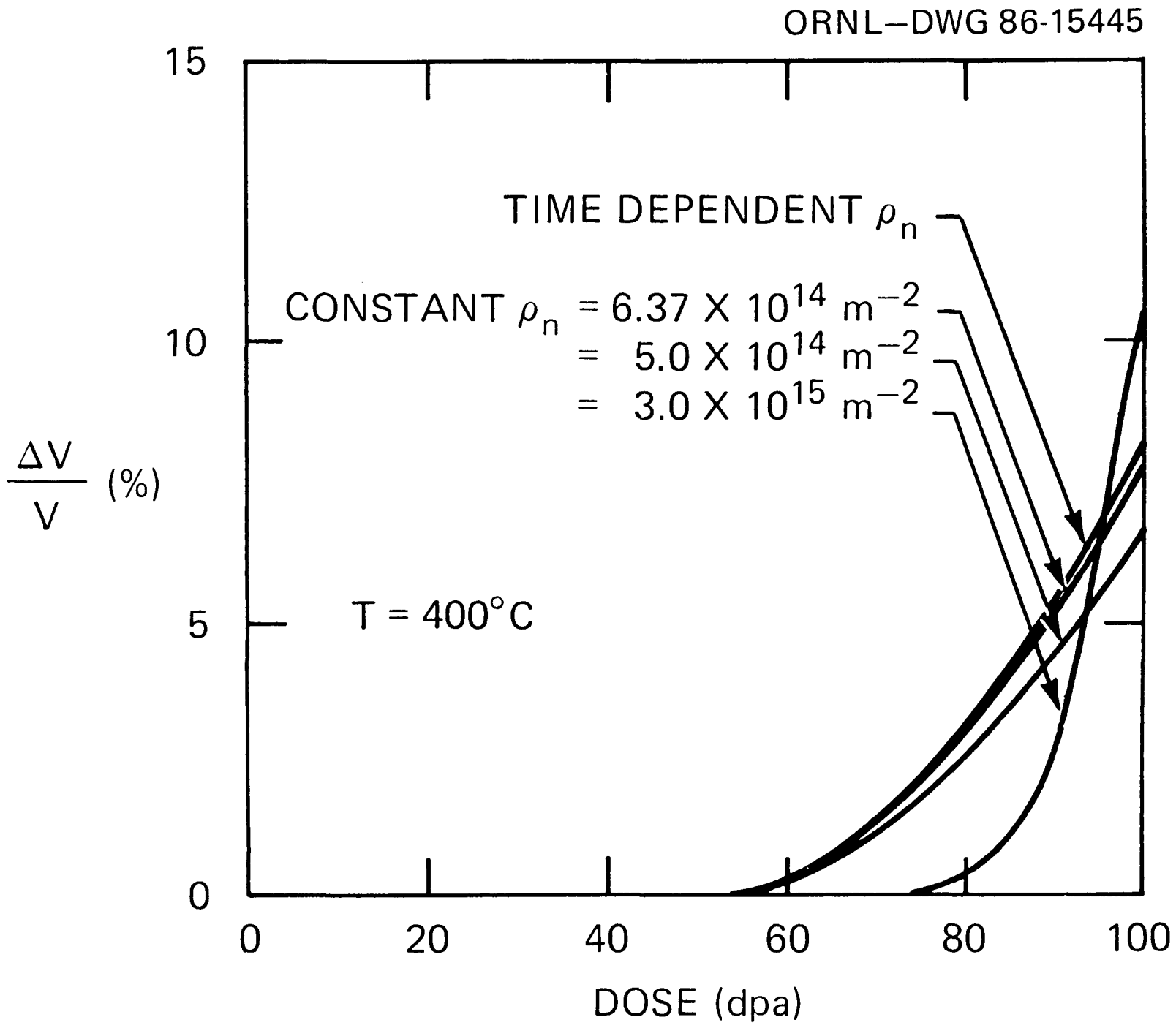

Fig 4.a
Stoller

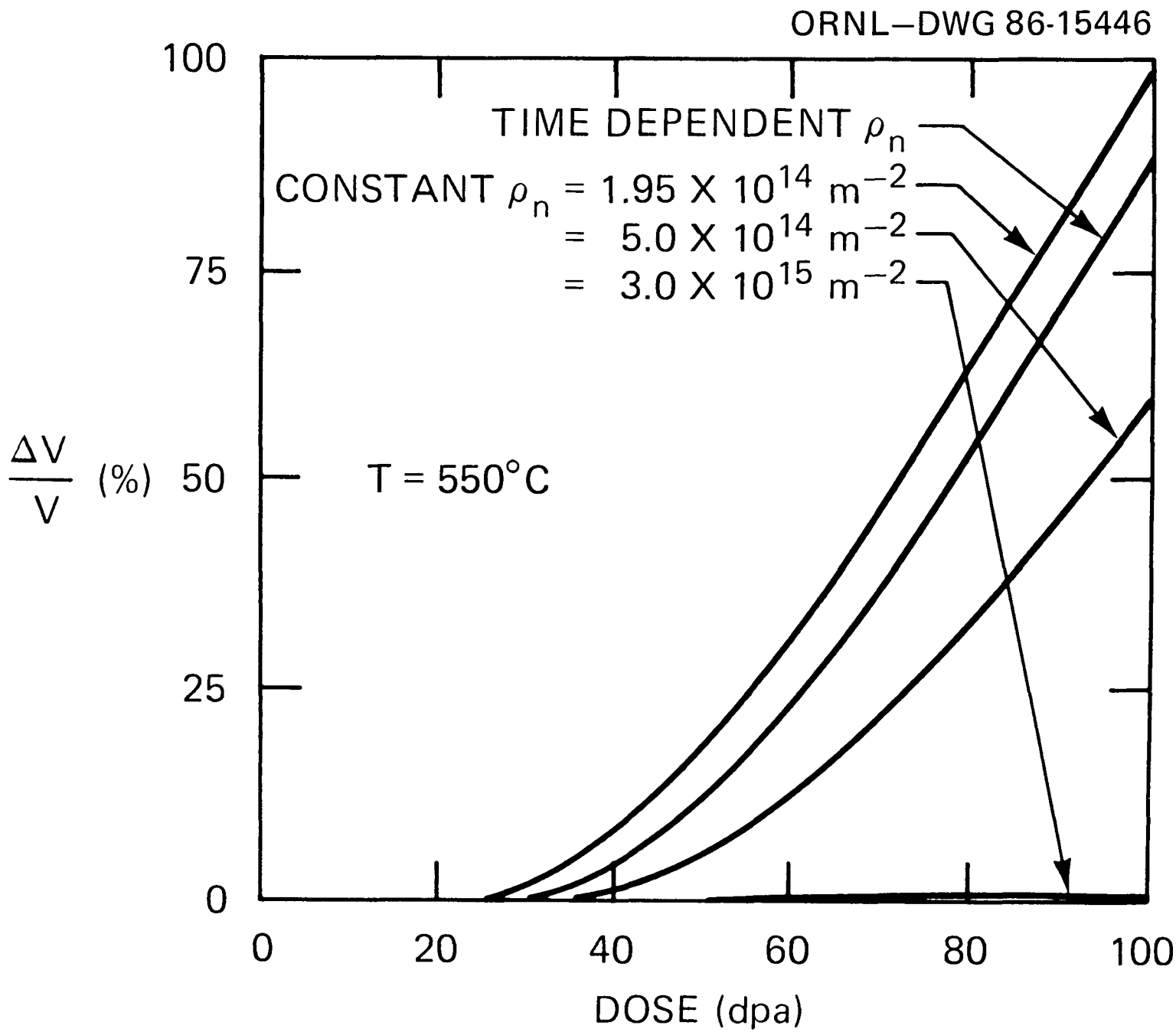

Fig 4b
Stoller

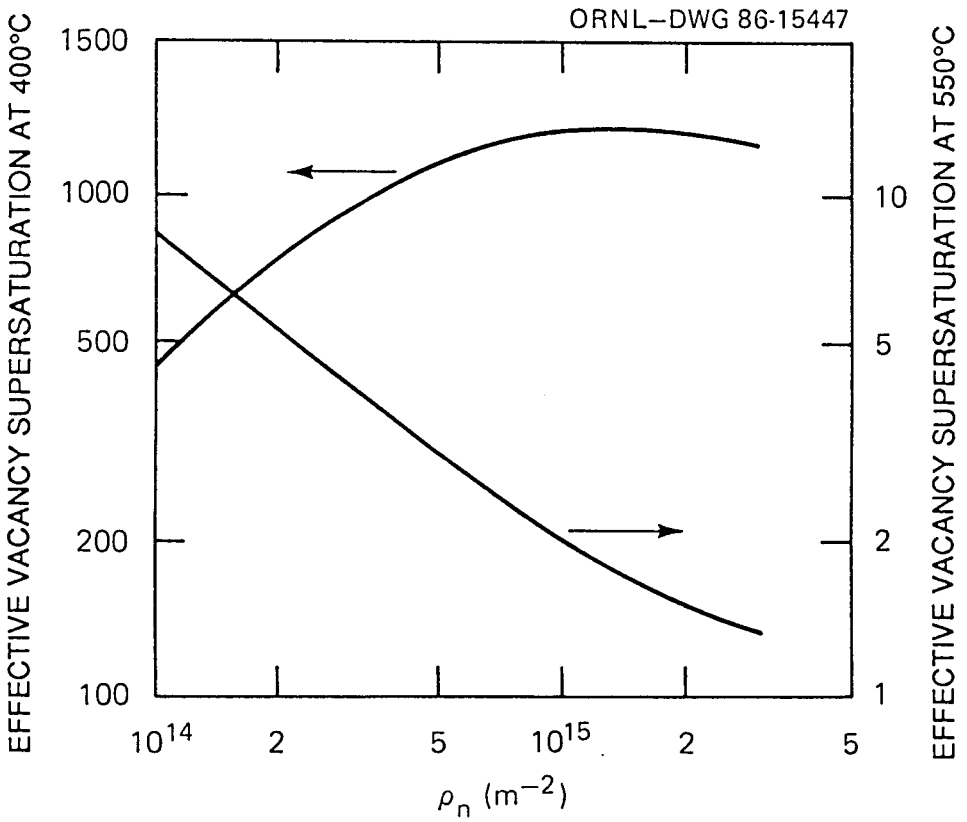

Fig 5
Stoller

ORNL-DWG 89Z-15934

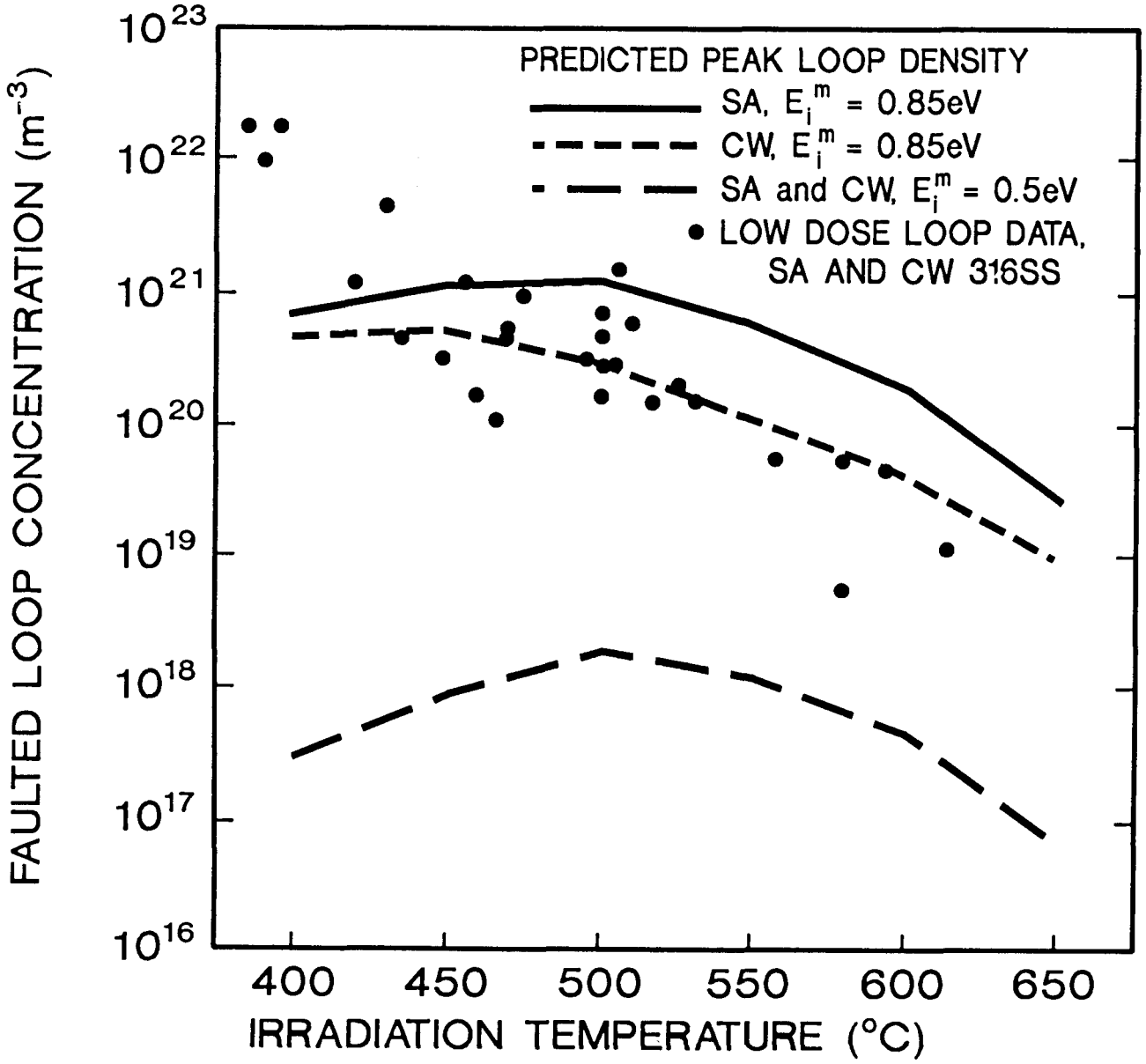

Fig. 6a
Stoller

ORNL-DWG 89Z-15935

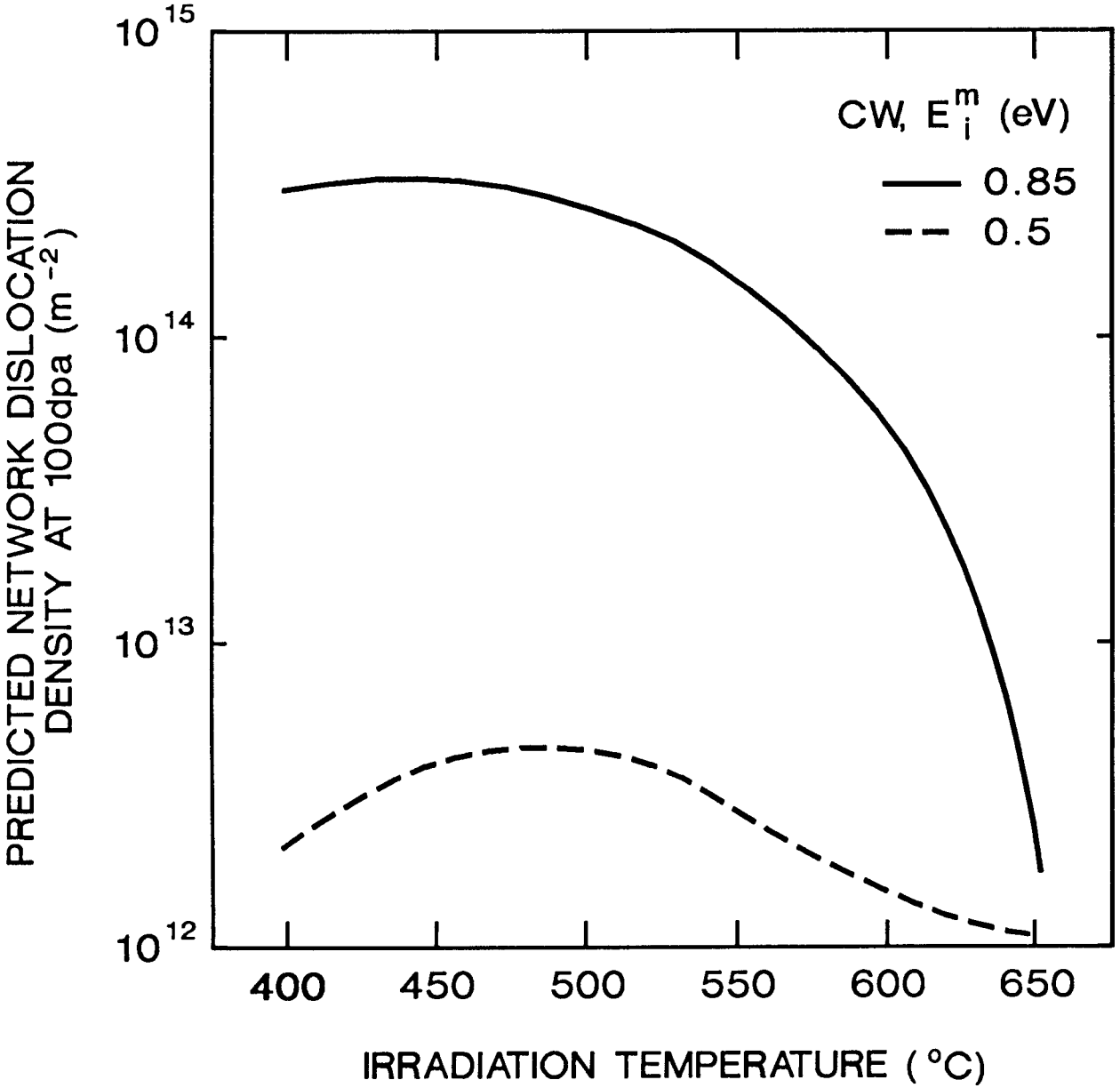

Fig. 6b
Stoller

ORNL-DWG 89Z-15933

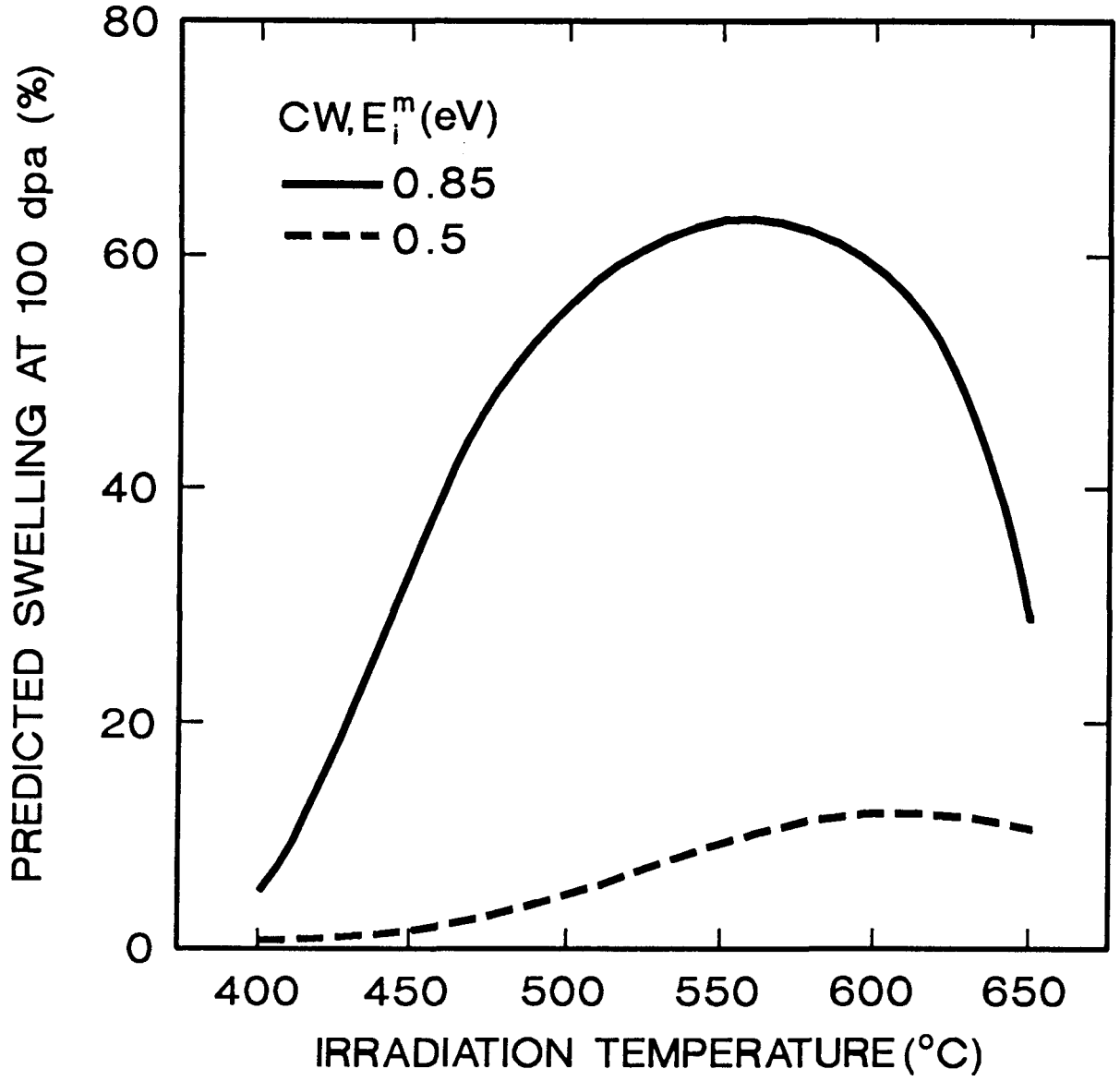

Fig. 6c
Stoller

ORNL-DWG 85-16840

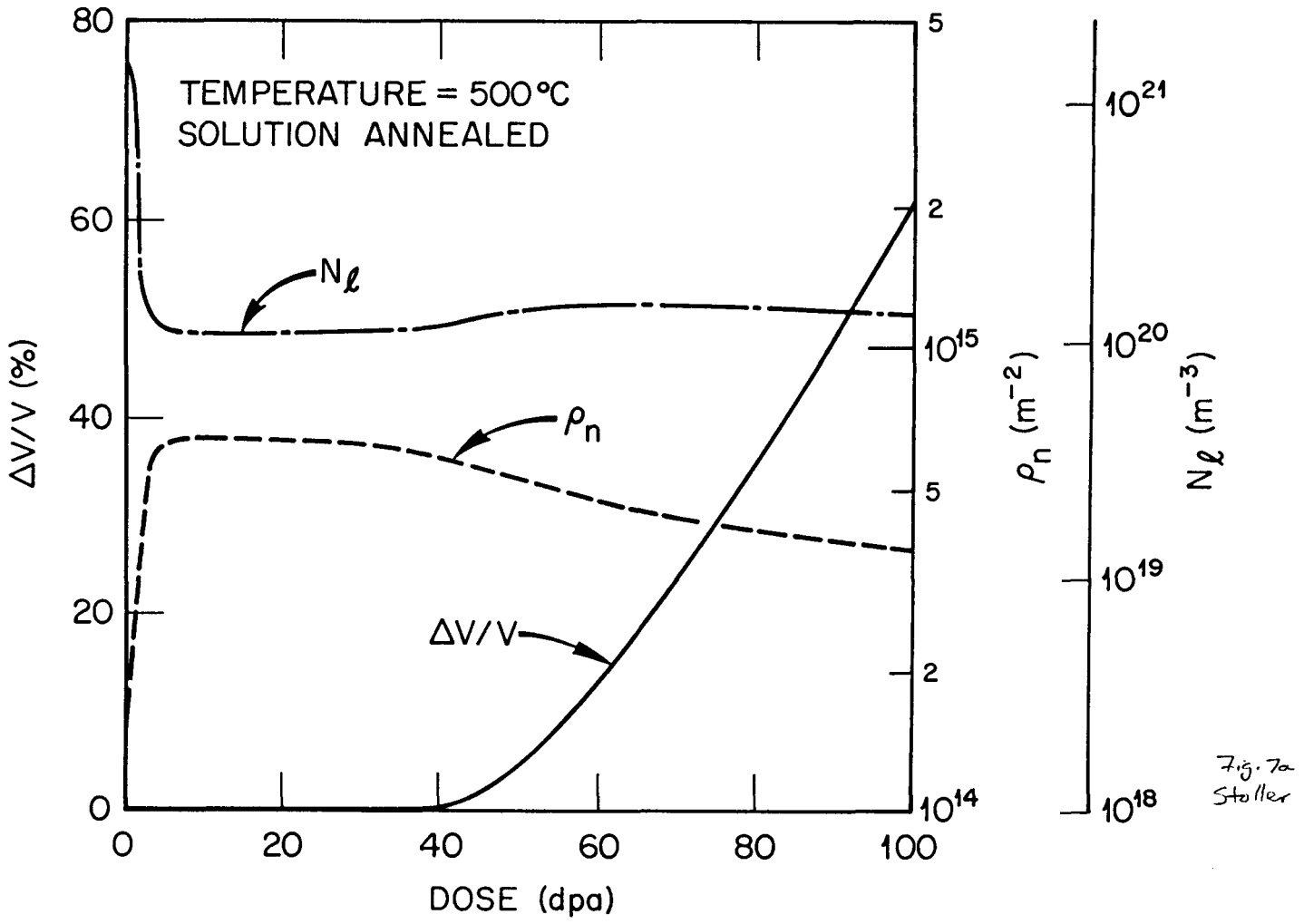

Fig. 7a
Stoller

ORNL-DWG 85-16839

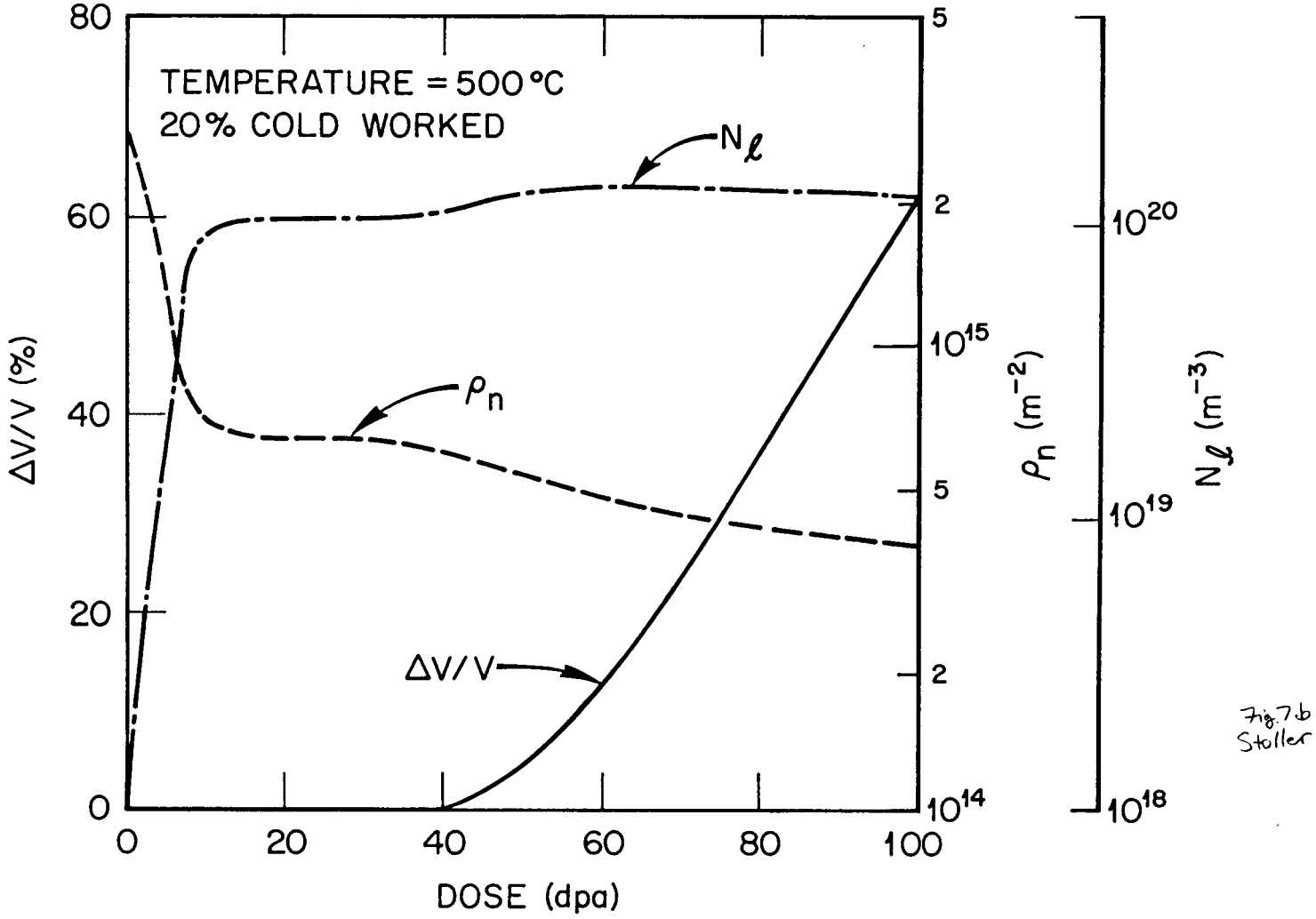

Fig. 7b
Stoller